Debris Attitude Motion Measurements and Modelling by Combining Different Observation Techniques

Principal Jiří Šilha[(1)], T. Schildknecht[(1)], J.-N. Pittet[(1)], G. Kirchner[(2)], M. Steindorfer [(2)], D. Kucharski[(2)], D. Cerutti-Maori[(3)], J. Rosebrock[(3)], S. Sommer[(3)], L. Leushacke[(3)], P. Kärräng[(4)], R. Kanzler[(4)], H. Krag[(5)]

[(1)] Astronomical Institute, University of Bern, Sidlerstr. 5, CH-3012 Bern, Switzerland, Email: jiri.silha@aiub.unibe.ch
[(2)] Space Research Institute of the Austrian Academy of Sciences, Lustbuehelstrasse 46, A-8042 Graz, Austria, Email: georg.kirchner@oeaw.ac.at
[(3)] Fraunhofer Institute for High Frequency Physics and Radar Techniques, Fraunhoferstraße 20, 53343 Wachtberg, Germany, Email: delphine.cerutti-maori@fhr.fraunhofer.de
[(4)] HTG - Hyperschall Technologie Göttingen GmbH, Albert-Einstein-Str. 11, D-37191 Katlenburg-Lindau, Germany, Email: r.kanzler@htg-hst.de
[(5)] ESA/ESOC, Space Debris Office, Robert-Bosch-Straße 5, DE-64293 Darmstadt, Germany, Email: holger.krag@esa.int

ABSTRACT

This work will discuss an ESA project "Debris Attitude Motion Measurements and Modeling" (ESA AO/1-7803/14/D/SR) dedicated to the attitude determination of large spacecraft and upper stages. Two major goals are defined for this project. First, the determination of the attitude motion vector in case of a contingency situation, when a short response time is required between the observations themselves and the attitude determination. The second goal is the long term prediction (e.g. 10 years) of the spin rate of selected targets for future potential Active Debris Removal (ADR) missions. The study should in particular fuse the results from passive optical, laser ranging and radar observations.

We will discuss a highly modular software tool named ιOTA (In-Orbit Tumbling Analysis) which was developed during the presented activity. This tool performs short- (days) to long-term (years) propagations of the orbit and the attitude motion of spacecraft in Earth orbit and furthermore its post-processing modules will generate synthetic measurements, i.e. light curves, satellite laser ranging (SLR) residuals and synthetic radar images.

Last but not least we will present results from a collaborative campaign when four priority targets have been selected for collaborative measurements with radar, SLR and light curves in order to test and validate the IOTA tool.

1 INTRODUCTION

The population of space debris increased drastically during the last years. Catastrophic collisions involving massive objects produce large number of fragments leading to significant growth of the space debris population. An effective remediation measure in order to stabilize the population in Low Earth Orbit (LEO) is therefore the removal of large, massive space debris. Secondly, satellite malfunctions might lead to loss of contact with the spacecraft and an accurate attitude determination can help to identify the cause. Such scenarios are referred to as contingency cases.

Currently, the Astronomic Institute of the University of Bern (AIUB) in cooperation with three partners is involved in an ESA study Debris Attitude Motion Measurements and Modelling (ESA AO/1-7803/14/D/SR) dedicated to the attitude determination of large spacecraft and upper stages. One of the project consortium partners, Hypersonic Technology Goettingen (HTG), is developing a highly modular software tool ιOTA to perform short- (days) to long-term (years) propagations of the orbit and of the attitude motion of a spacecraft, taking into account all the relevant acting forces and torques [1]. Furthermore, ιOTA's post-processing modules will generate synthetic measurements, e.g. light curves, Satellite Laser Ranging (SLR) residuals and Inverse Synthetic Aperture Radar (ISAR) images that can be compared with the real measurements. The strength of the approach is the combination of various attitude measurement types to cancel out ambiguities of the individual methods and to combine this information with a dynamic model in order to establish attitude prediction. The validation of the attitude model will be done by comparison to real observations of targets with known attitude. For more about the ιOTA tool please refer to [1].

2 IN-ORBIT TUMBLING ANALYSIS TOOL

ιOTA is a standalone tool programmed in C++. One of the key features of the software is the approach of high modularity for the simulation of the relevant effects, as well as regarding the used environmental models, enabling easy updates of existing models and an easy

implementation of new models released. Except for the gravitational influence of the Earth, the user will be able to choose which particular effects shall be included in the simulation.

2.1 Modular architecture design

The ιOTA host process calls the particular submodules of the software. Fig. 1 displays the decomposition of the software, including the software modules, the data flow from the model and input data (blue) to the particular modules, as well as the data flow from the simulation (yellow) and propagation (red) modules to the particular destination. The post processing branch (green) provides the final processing and visualization of the simulation results.

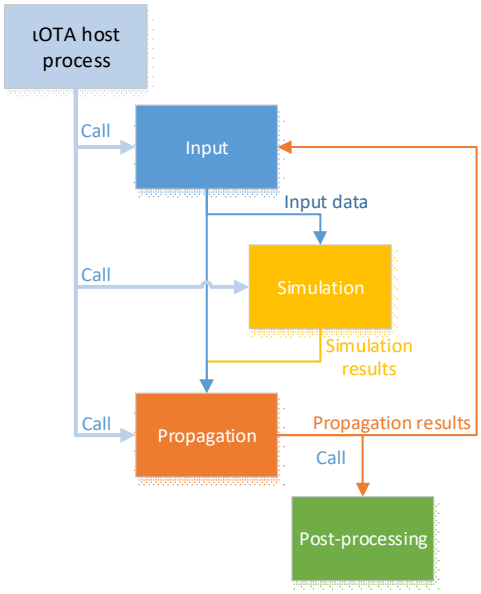

Figure 1. ιOTA process hierarchy and functional architecture [1]

The simulation part of ιOTA is called from the command line. Before running the software, the simulation setup needs to be defined by the user via configuration files.

The environmental conditions for the attitude simulation comprise the modelling of forces and torques resulting from atmospheric drag, gravitational influences from Earth, Sun and Moon, eddy current damping caused by the tumbling motion inside the Earth's magnetosphere, solar radiation pressure and impulse transfer through user defined micrometeoroid and small space debris impact events. Simulation modules for environmental influences are

- Aerodynamics forces and torque
- Eddy current damping
- Gravitational acceleration and torque (Earth)
- Impact events
- Solar radiation pressure
- Third-body acceleration (Sun and Moon)

Simulation modules for optional spacecraft related influences are

- AOCS behaviour: Magnetic torquer activation
- AOCS behaviour: Reaction wheel behaviour
- AOCS behaviour: Thruster firing
- Moving parts (tank sloshing)
- Outgassing or leakage

Except for the tank sloshing, these internal effects are managed through user defined events.

The post-processing modules comprise

- History module: Output and storage of all relevant (selected) simulation data
- Light curve modelling
- Optical image generation in the GUI
- Radar image generation and Radar Cross Section estimation
- Satellite laser ranging measurement simulation

The post processing is done during the simulation, providing accessible results to the user while the simulation is running. Using the ιOTA-GUI, the user can visualize the simulation results, i.e. history data for the orbit and attitude motion, as well as acting forces and torques and the synthetic measurements generated.

2.2 Simulation input and modelling

Mandatory input for the simulation is the initial spacecraft orbit and attitude, as well as the epoch. Also a surface geometry model of the spacecraft, based on triangular panels, as shown in Fig. 2 for the ENVISAT satellite (international designator 2002-009A) taken from [2], has to be provided by the user. The spacecraft mass, moments of inertia (MoI) and the center of mass (CoM) position within the surface geometry model have to be defined by the user.

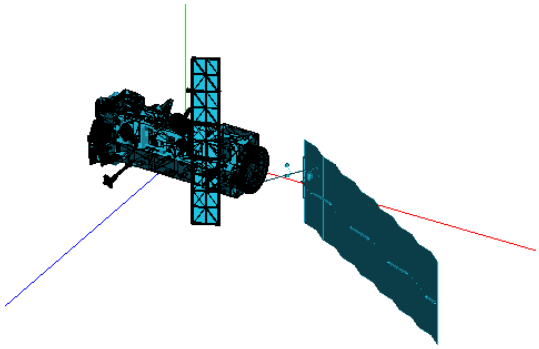

Figure 2. ENVISAT 3D model used in ιOTA [2]

The input parameters are

- the attitude state assumption based on real observations, e.g. initial values for spin rate and spin axis direction determined from SLR

data, from direct imaging or from SAR images,
- environmental conditions,
- the 3D surface geometry/shape of the target,
- the CoM determined from International Laser Ranging Service (ILRS) network data or Doppler Orbitography and Radio-positioning Integrated by Satellite (DORIS) measurements or obtained from models,
- the MoI obtained from the manufacturer data or models,
- the surface properties, diffuse and specular reflection,
- the retro-reflector positions according to the CoM and to the surface geometry.

3 OBSERVATION TECHNIQUES

The attitude states of space objects can be estimated by using several types of measurement and with them related methods. Some of them can provide direct information about the object spin behavior, like SLR measurements to cooperative targets [3], [4] or Inverse Synthetic Aperture Radar (ISAR) images performed by radar [5]. Direct optical imaging [6] after processing may provide similar results as the ISAR images. Most cost effective for long term monitoring of the objects behavior and its changes are the optical telescope measurements, when a light curve of the object is acquired. By applying time series analysis tools one can extract the rotational frequencies from light curves [7].

3.1 Optical passive measurements

For targets, such as rotating spacecraft, upper stages, and debris pieces, a sequence of photometric measurements is acquired within a short time interval (few minutes) with a small time step (few seconds), depending on the orbit and attitude of the target. The output of such a sequence, i.e. the brightness variation during the measurement time is a so-called light curve. Light curves are strongly related to the rotation of the observed object. To be able to analyze light curves obtained by optical measurements, i.e. determining the rotation period and the rotation axis direction, several methods can be applied [7]. Example of a light curve for GLONASS satellite 2001-053C acquired by AIUB's ZIMLAT system (see section 4.1) is plotted in Fig. 3.

For more about the space debris light curves acquisition and processing please refer to [7].

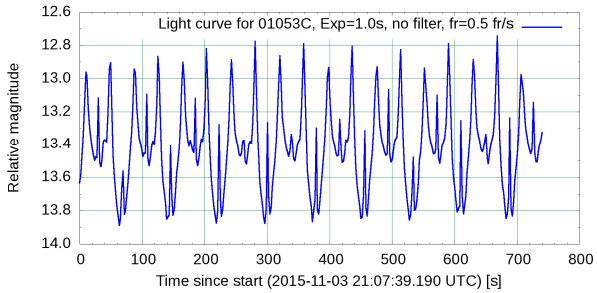

Figure 3. Light curve for GLONASS satellite 2001-053C acquired by AIUB's ZIMLAT system

3.2 Radar measurements

3.2.1 ISAR principle

Advantages of radar systems compared to other measurements systems like optical systems are their ability to observe space objects at any time a day independently from the weather conditions.

Inverse synthetic aperture radars (ISAR) exploit the rotational motion between radar and object in order to image the object in 2D. The radar transmits regularly waveforms that are backscattered by the object and received by the radar. From the delay between transmit and receive, the ranges between the radar and the different point scatterers, which are distributed over the object, can be measured. Over time, the object rotation causes small variations of these distances. This induces phase differences between radar pulses that are proportional to cross-range (i. e. direction perpendicular to range). Cross-range positions can therefore be separated by spectral analysis of consecutive pulses.

Challenge of ISAR imaging is the estimation of the unknown object motion from the radar data. Indeed, the kinematics of the object is required in order to form a focused image of the moving object. The motion of the object can be decomposed into a translational motion of a reference point of the object, which has to be compensated, and a rotational motion around an axis through this reference point, which leads to ISAR imaging.

The object is imaged in the so called image plane. The first direction (range) is in the line-of-sight (LOS) direction from the radar to the object. The second direction (cross-range) is determined by the effective rotation vector, which is the projection of the rotation vector of the object (w.r.t. a coordinate system aligned with the LOS) orthogonal to the LOS vector. The norm of the effective rotation vector scales the ISAR images in cross-range. The image plane is,hence, the range / cross range plane that is perpendicular to the effective rotation vector and contains the LOS vector. The scatterers of the object are projected to this image plane spanned by the moving LOS.

Unfortunately, the image plane and the cross-range scaling of an ISAR image are changing with time and are usually unknown. They depend on the satellite's rotational motion, the satellite's orbit, the radar location and Earth rotation. All, except for the first parameter, are usually known in advance. Therefore, correct cross-range scaling can only be obtained if the rotational motion of the object, i.e. the sequence of its attitudes over time, is known or has been estimated.

3.2.2 Attitude estimation from ISAR images

Two different parametric methods were developed to estimate the rotational motion from a sequence of ISAR images. Both methods enable the rotational velocity vector to be estimated for both slowly and fast tumbling objects with ground-based imaging radars.

Parametric attitude estimation requires a suitable rotational motion model. The two methods are based on different models. The first method assumes a constant rotation vector (whose length is the rotational velocity and whose direction is the axis) in an inertial system over one satellite pass. The second method uses the simulation tool ιOTA, which simulates the temporal evolution of attitude. In both cases, the initial state is given by the attitude and the rotation vector at reference time.

The two methods use a wire-grid model (WGM) of the satellite, which is projected to the ISAR images. The projections of the WGM corners can then be compared to salient points in an ISAR image. Knowing the satellite's attitude over time, the image plane and cross-range scaling for several images of a passage can be computed.

3.2.2.1 First optimization procedure

Fig. 4 shows the optimization procedure under the assumption of a fixed rotational velocity vector over a satellite pass. It is based on a maximum likelihood (ML) approach. Attitude estimation is accomplished by estimating the parameters of a rotational motion model. First the WGM is projected manually on a few ISAR images. Then, for a given initial attitude and a rotational velocity vector, the WGM is automatically projected on the ISAR image sequence. The algorithm searches for the parameters that match best the automatic projections with the manual projections.

The quality of matching is expressed by an error measure. We took the mean of squared distances between projected corners and assigned image points for this purpose. An alternative error measure was also investigated. If a proper rotation and cross-range scaling of the WGM is found by matching the image content, this rotation can be compared to the rotation predicted by the rotational motion model for given parameters. Both rotations can be described by a rotation vector. The alternative error measure is then the squared Euclidean distance of both vectors.

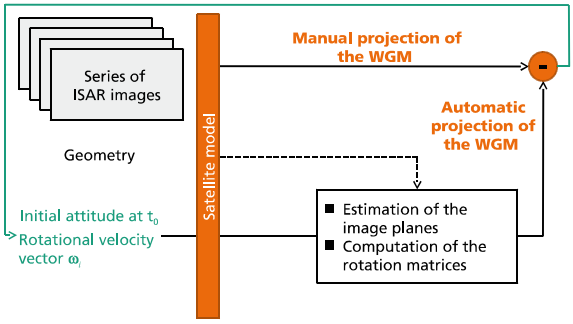

Figure 4. Optimization without ιOTA

3.2.2.2 Second optimization procedure (with ιOTA)

ιOTA propagates an initial state over time by computing location and attitude. Since the translational motion is also simulated, the initial state, defined by position and velocity of the satellite, has to be specified additionally. This state is usually known in advance. A single 6-dimensional optimization procedure is applied, which is illustrated in Fig. 5.

ιOTA computes the satellite's attitude relative to the Earth centered inertial (ECI) system as a function of time resulting in the current rotational velocity vector in ECI coordinates. The satellite's orbital position and the radar location as functions of time yield the temporal evolution of the LOS direction in ECI coordinates. This corresponds to rotation of the ECI system relative to a coordinate system where one coordinate permanently points in LOS direction. Subtracting both rotations yields the LOS rotational velocity vector relative to the satellite, given in ECI coordinates. Cross-range is orthogonal to both this vector and the LOS. Thus, the image plane is defined as well as cross-range scaling.

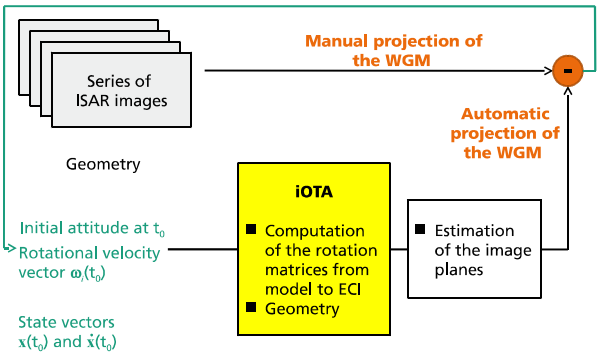

Figure 5. Optimization with ιOTA

3.3 SLR measurements

SLR is a technique measuring the time of flight of laser photons between a ground-based observatory and a satellite. SLR is usually performed to objects equipped with retro-reflector array (RRA), also known as

cooperative targets. SLR measurements themselves can directly provide two types of data related to the attitude state, where both are related to the rotation of satellite's RRA around its center of mass (CoM). First type, is the modulation on the range between the laser and the object's RRA. The second type of data is the alternative visible or hidden state of the RRA viewed from the observatory. An example of a SLR residuals acquired by Space Research Institute's (IWF from German Institut für Weltraumforschung) Graz SLR station (see section 4.3) can be seen in Fig. 6.

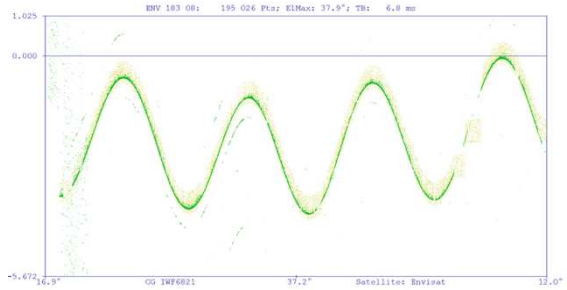

Figure 6. SLR residuals of ENVISAT measured by Graz SLR station

4 SENSORS

Within this study several different sensors have been used to acquire attitude related measurements to space debris objects.

4.1 ZIMLAT telescope

One of the main instruments at AIUB's at the Swiss Optical Ground Station and Geodynamics Observatory Zimmerwald, Switzerland (hereafter Zimmerwald observatory) (observatory code 026, SLR station code ZIML) is 1-meter Zimmerwald Laser and Astrometry Telescope (ZIMLAT). ZIMLAT is used either for SLR to cooperative targets, targets equipped with SLR retroreflectors, or for optical observations (astrometric positions and magnitudes) of artificial and natural objects in near-Earth space. During daytime the system operates in SLR mode only. During the night time the available observation time is shared between SLR and CCD/sCMOS [8] based on target priorities. The switching between the modes is done under computer control and needs less than half a minute. ZIMLAT telescope is shown in Fig. 7.

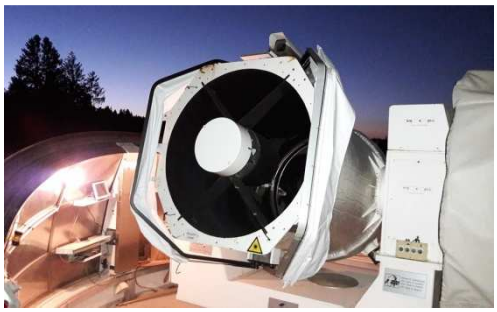

Figure 7. AIUB's ZIMLAT telescope. Photo credit: Silha and Bodenmann, 2016

4.2 TIRA radar

The space observation radar TIRA (Tracking and Imaging Radar) located in Germany is the largest experimental system which is unique in Europe. It is operated by the Fraunhofer Institute for High Frequency Physics and Radar Techniques FHR. The system primarily serves as the central experimental facility for the development and investigation of radar techniques for the detection and reconnaissance of objects in space. TIRA also provides valuable support for space missions: space agencies from all over the world use the special capabilities of the FHR scientists and their system. As the name implies, the TIRA system comprises a tracking radar and an imaging radar. The narrowband, fully coherent, high power tracking radar has a transmission frequency in L-band (1,333 GHz) and the wideband imaging radar has a transmission frequency in Ku-band (16.7 GHz) and is currently equipped with a high target resolution. TIRA radar is shown in Fig. 8.

Figure 8. FHR's TIRA system. Photo credit: Fraunhofer FHR

4.3 Graz SLR station

The IWF's Graz SLR station (station code GRZL) is housed in the Observatory Lustbuehel, Austia. In order to test laser ranging possibilities to space debris objects,

the Satellite Laser Ranging (SLR) Station Graz installed 2012 a frequency doubled Nd:YAG pulse laser with a 1 kHz repetition rate, a pulse width of 10 ns, and a pulse energy of 25 mJ at 532 nm (on loan from German Aerospace Center Stuttgart, DLR). This laser was replaced in 2013 by another frequency doubled Nd:YAG pulse laser with 100 Hz repetition rate, a pulse width of 3 ns, and a single pulse energy of 200 mJ at 532 nm, also on loan from DLR Stuttgart.

Additionally, the station is able to acquire single-photon light curves recording to cooperative and non-cooperative targets [9].

The Graz SLR system is plotted in Fig. 9.

Figure 9. IWF's Graz Laser Telescope dome at Observatory Lustbuehel, Austria, Photo credit: IWF

5 TARGET LIST

We defined five priority targets to be observed during simultaneous observations. Because of the high interest, ENVISAT (2001-002A), a former ESA satellite which is non-active since 2012, have been selected as priority target. In 8th of April 2012 the Agency lost contact with the satellite. Currently, ENVISAT is one of the largest and heaviest objects in Low Earth Orbit (LEO) region, which is the highest dense region, and can pose a big treat in case of collision or break-up event. ENVISAT is on mean orbital altitude around 766 km. It is equipped with RRA which makes is observable by any SLR system if RRA is visible from the station. The 3D model of ENVISAT satellite used in ιOTA tool is plotted in Fig. 2.

We selected former ESA missions ERS-1 (1911-050A) and ERS-2 (1995-021A) (Fig. 10, left panel) as other two priority targets. ERS-1 mission ended in 2000 after 9 years of service by failure on board attitude control system. Satellite is currently on LEO orbit with mean altitude around 770 km. ERS-2 was decommissioned in 2011 and its orbit has been lowered from 750 km to 573 km to decrease satellite lifetime. Both ERS satellites are equipped with RRA and have a very similar design.

Fourth selected target was ADEOS-2 (2002-056A) (Fig. 10, right panel), a former Japan Aerospace Exploration Agency (JAXA) mission. ADEOS-2 was launched in 2002 on LEO orbit with mean orbital altitude around 800 km. After one year of service the mission ended by the failure of the solar panel. Since then the satellite showed several sudden accelerations in rotations. The most current one was observed by ZIMLAT system in December 2015.

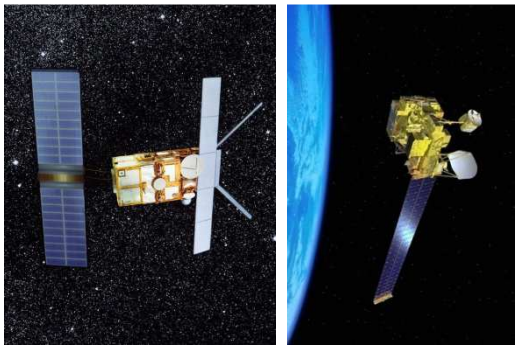

Figure 10. Satellites ESA ERS-2 (left panel) and JAXA ADEOS-2 (right panel), Photo credit: ESA and JAXA

Our last target selected was JAXA upper stage H-2A R/B (2001-038B). This is the only object which is placed on orbit outside LEO, namely on highly eccentric orbit with perigee and apogee altitudes of ~260 km and 34,180 km, respectively. The vehicle evaluation payload (VEP-2) was launched in 2001 for testing purposes and has been observed several times by radars since then, e.g. by TIRA. The H-2A R/B is plotted in Fig. 11.

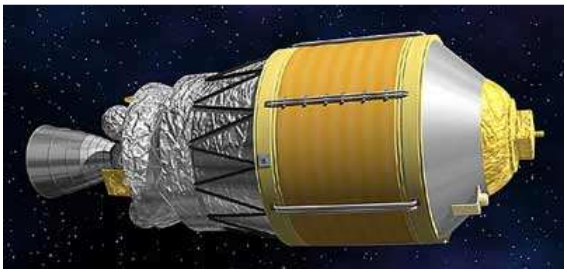

Figure 11. Upper stage H-2A R/B, Photo credit: JAXA

6 SOFTWARE VALIDATION

Several different modules need to be validated for ιOTA, namely synthetic measurements generation and modelling of acting torques and forces. Below are examples of such validations.

6.1 Light curves, Jason-3 case

During the night 2017-03-15 we acquired with ZIMLAT telescope a light curve of active satellite Jason-3. The whole pass from satellites ascending to descending point has been covered. The obtained light curve is plotted in Fig. 12, red points. As expected the light curve showed a relatively simple change of rightness over time, mostly function of the object elevation over the horizon. No apparent satellite rotation is visible in the light curve.

For the same pass we generated synthetic light curves by using ιOTA, the Jason-3 3D model available by NASA and by assuming different reflective properties for the satellite surface (ratio between diffusely and specular reflected ligth). All the generated light curves are plotted in Fig. 12. To get a good match between the real and synthetic light curves we had to add a time shift of 150 s to the real light curve. This discrepancy will be further investigated. The vertical axis (magnitude) for the real light curve is in a relative scale and has not been calibrated. Once shifted, the shape of real light curve is in good match with the light curves created by diffusely reflected light.

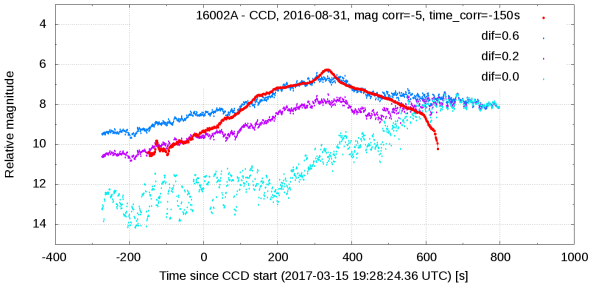

Figure 12. Light curve of attitude-controlled Jason-3 satellite acquired by ZIMLAT system during night 2017-03-15 (red line) and synthetic light curves generated by ιOTA for the same pass assuming different diffuse factor

6.2 SLR residuals, ENVISAT case

In Fig. 13 is plotted an example of synthetic SLR ranges of ENVISAT generated by ιOTA (green points) in comparison with real SLR ranges (blue points) acquired by ZIMLAT telescope during the night 2016-08-22. The synthetic SLR residuals could be generated once we found a rotation angular velocity vector of ENVISAT during given pass by using ιOTA.

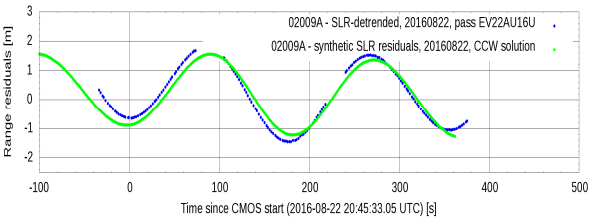

Figure 13. SLR residuals of ENVISAT satellite acquired by ZIMLAT system during night 2016-08-22 (blue points) and synthetic residuals generated by ιOTA for the same pass (green points)

6.3 Long-term prediction, ENVISAT case

In Fig. 14 is plotted one year evolution of ENVISAT's rotational velocity by assuming different acting torques and forces, namely eddy current, gravitational torque, 3rd body torque and all three types of torques combined. These values are compared to the angular velocities extracted from the ZIMLAT SLR residuals which were processed by AIUB [3]. Investigated was period of time between July 2013 to August 2014. As can be seen from Fig. 14 we have a good agreement between real extracted values and predicted values.

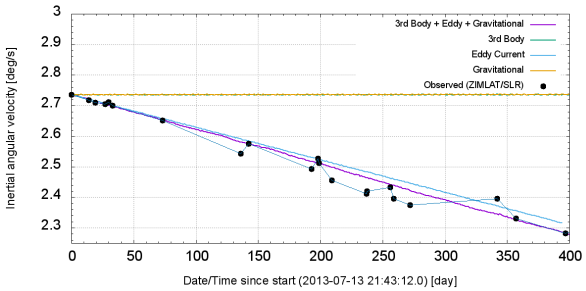

Figure 14. Inertial angular velocity of ENVISAT satellite determined by AIUB from the SLR residuals acquired by ZIMLAT system during years 2013 – 2014 (black points) and predicted angular velocity by assuming different acting torques/forces

7 COLLABORATIVE OBSERVATION CAMPAIGN

The goal of the collaborative observations was to observe the same target at the same time with different types of sensor. These measurements should suit for the exploration of the used methods cross-calibration and as a testing data for the ιOTA tool evaluation.

7.1 Observation nights selection

We have three sensors available for the observation campaign, TIRA, ZIMLAT telescope and Graz SLR station. From our five priority targets we selected only spacecraft of LEO. The H-2A R/B could not be observed by any other system than by ZIMLAT (light curve acquisition) due to its high altitude and absence of RRA.

We investigated visibilities of ENVISAT, ERS-1, ERS-2 and ADEOS-2 for time period between spring and winter 2016 for all three observation sites. For light curve it has to be valid that during the observation the object is illuminated by the sun while the sun is below horizon in order to decrease the background noise. We used following criteria for selecting the correct pass for the simultaneous measurements:

- All objects are illuminated by the sun
- All objects are above horizon for all stations, preferably > +30° for Zimmerwald station
- Sun is below horizon for Zimmerwald station, preferably -5°
- Objects are visible from all three sites for at least 3 minutes
- At least one pass of ENVISAT during given night fulfills previously listed criteria

Additionally, we included also following two criteria:

- TIRA is available
- Latest 24 hours before the observation campaign the weather predictions were favorable at least for Zimmerwald observatory or Graz SLR station

By following mentioned criteria we got one month of overlap when we could observe all four targets within one night from all three observation sites. Finally, we selected five nights for collaborative measurements, namely 2016-08-26, 2016-09-04, 2016-09-06, 2016-09-10 and 2016-09-21.

7.2 Observation campaigns

Due to the weather conditions, we performed collaborative measurements during nights 2016-09-06 and 2016-09-21. Unfortunately, the weather conditions at Graz SLR station prevent the station to perform observations during any of the mentioned nights. Therefore, used have been TIRA for ISAR imaging and ZIMLAT for simultaneous light curve and SLR acquisition. ZIMLAT light curve acquisition was performed either by using CCD camera, when frame-rate of about 0.75 frames/s was used or by sCMOS camera when a frame-rate of ~ 5.0 frames/s was used. The summary of the observations for nights 2016-09-06 and 2016-09-21 can be seen in Tab. 1 and 2, respectively.

Pass	AIUB SLR	Remark	AIUB LC	Remark	FHR	Remark
ENVISAT 2016-09-06 18:10 UTC	**N/A**	-	**N/A**	-	**YES**	L-band + Ku-band
ENVISAT 2016-09-06 19:47 UTC	**YES**	~400 Interrupted signal	**YES**	CMOS ~400s	**YES**	L-band + Ku-band
ERS-1 2016-09-07 01:43 UTC	**NO**	-	**YES**	CMOS ~250s	**YES**	L-band + Ku-band
ERS-2 2016-09-07 01:51 UTC	**NO**	-	**YES**	CMOS ~120s	**-**	-
Adeos-2 2016-09-07 03:09 UTC	**NO**	-	**YES**	CMOS ~450s	**YES**	L-band + Ku-band
ERS-2 2016-09-07 03:23 UTC	**N/A**	-	**YES**	CCD ~130s	**YES**	L-band + Ku-band

YES – acquisition was successful, data are available, NO – Applicable only for SLR. Attempt to acquire data but un-successful, (N/A) – No attempt.

Table 1. Summary of simultaneous observations performed during night 2016-09-06

Pass	AIUB SLR	Remark	AIUB LC	Remark	FHR	Remark
ENVISAT 2016-09-21 18:57 UTC	**NO**	-	**YES**	CMOS ~200s	**YES**	L-band + Ku-band
ENVISAT 2016-09-21 20:37 UTC	**YES**	~500s Full signal	**YES**	CMOS ~120s	**YES**	L-band + Ku-band
ERS-1 2016-09-22 00:57 UTC	**N/A**	-	**N/A**	-	**YES**	L-band + Ku-band
ERS-2 2016-09-22 02:13 UTC	**NO**	-	**YES**	CMOS ~50s	**YES**	L-band + Ku-band
ERS-1 2016-09-22 02:39 UTC	**NO**	-	**YES**	CMOS ~100s Interrupted	**YES**	L-band + Ku-band
Adeos-2 2016-09-22 03:25 UTC				~450s		Ku-band

YES – acquisition was successful, data are available, NO – Applicable only for SLR. Attempt to acquire data but un-successful, (N/A) – No attempt.

Table 2. Summary of simultaneous observations performed during night 2016-09-21

7.3 Acquired measurements, TIRA

The results were obtained with data acquired with the Tracking and Imaging Radar (TIRA) of Fraunhofer FHR [10,11].

7.3.1 Attitude estimation with ιOTA

Attitude estimation using the simulator ιOTA needs much more computational power than assuming a fixed rotational velocity vector in the inertial system (several hours for the optimization with ιOTA vs. less than a minute for the optimization without ιOTA). Therefore, only one passage of ENVISAT was analysed by this method (see [5] for the temporal investigation of ENVISAT's rotational motion using the first optimization procedure). Fig. 14 shows ISAR images of ENVISAT with overlaid WGMs. For testing purposes, first a CAD model of a sphere and a corresponding inertia tensor proportional to the unit matrix were applied. Doing so, the ιOTA result essentially gave the same mean square error (MSE) as the algorithm designed for a constant rotational velocity vector, and the initial attitude and rotational velocity vector differed only slightly. This confirmed the ιOTA simulation program. Comparing the attitude quaternions generated by ιOTA for subsequent time instances, it could be observed that the rotational velocity vector simulated by ιOTA kept nearly constant as expected for a spherical object.

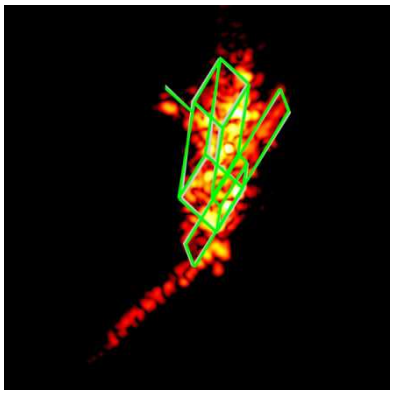

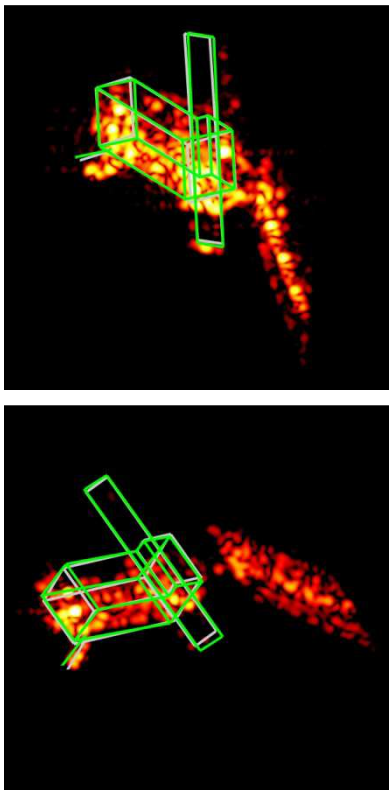

Figure 14. ISAR images of ENVISAT with superposed WGMs (green: manual projection, grey:automatic projection) after the optimization procedure

In a next step, the sphere was replaced by an ENVISAT CAD model along with the corresponding inertia tensor. Several error minimization procedures were tested. First, the estimate for constant rotation vector was taken for initialization. Then, random initialization was tried, leading in one case to an error reduction. The alternative error measure was also used in other cases as shown in Table 3. Using this measure led to similar results as the original one. Surprisingly, the original error measure was reduced by using the alternative error measure for minimization. The error measure could be further reduced by taking the result as initialization of subsequent error minimization with the original error measure. The resulting root mean square (RMS) position errors are given in Table 3.

All results refer to a minimization where WGM projections due to WGM matching to single images were taken as reference points in the image. Unexpectedly, for all procedures using iOTA the RMS error was higher than the RMS error for the constant rotational velocity assumption. The reason for this is not yet clear. A possible cause could be that the CAD model and/or its center of gravity and inertia tensor do not sufficiently match reality. Alternatively, the algorithm may not converge to the absolute minimum of the error function but to a relative minimum.

Physical model for optimization	**Initialization**	**RMS position error [m]**
constant rotation vector	random	0.14368
iOTA with error from all projected WGM points	initialized by constant rotation vector result	0.31906
iOTA with error from all projected WGM points	random, 4 trials	0.76028 2.52654 0.26897 0.78320
iOTA with alternative error measure	constant rotation vector result	0.23773
iOTA	Result from previous case	0.20102

Table 3: RMS error of point positions for different simulation and computation procedures.

7.3.2 Attitude estimation without iOTA

Table 4 gives the estimated velocity vectors for the different radar observations under the assumption of a constant rotation vector. ISAR images of the different objects are shown in Fig. 15.

While the WGM for ENVISAT was derived from a CAD model, the WGMs for the other satellites were derived by hand from data sheets provided by ESA. Therefore these WGMs might be inaccurate.

The assumption of constant rotation vector appears to be satisfied for all ENVISAT and ERS-1 passes. For ERS-2, this assumption seems to be satisfied only for the pass on 22 Sept. 2016. The pass on 07 Sept. 2016 was divided in 3 sub-passes. Individual rotation velocity vectors were fitted under the assumption of constant rotation vector over each sub-pass.

ADEOS-2 is a strongly tumbling object and the assumption of constant rotation velocity vector is not fulfilled. Therefore, it was not possible to derive a rotation vector from both passages.

Pass	Rotation vector [rad/s]			Rotational velocity [deg/s]
ENVISAT2016-09-0618:11 UTC	2.55e-02	1.16e-02	-1.60e-03	1.6066
ENVISAT2016-09-0619:48 UTC	2.64e-02	1.16e-02	3.85e-03	1.6683
ERS-12016-09-0701:43 UTC	8.92e-03	4.48e-03	-5.53e-03	0.6540
ERS-22016-09-0703:24 UTC	3.51e-03 8.57e-03 4.71e-03	-2.79e-03 -5.16e-04 -1.65e-03	-6.96e-03 1.41e-02 5.57e-03	0.4743 0.9896 0.4282
Adeos-22016-09-0703:09 UTC	NO			NO
ENVISAT2016-09-2118:53 UTC	1.94e-02	2.12e-02	8.69e-04	1.6498
ENVISAT2016-09-2120:32 UTC	1.52e-02	2.43e-02	1.93e-03	1.6442
ERS-12016-09-2200:54 UTC	-1.29e-02	3.62e-03	1.45e-03	0.7700
ERS-22016-09-2202:10 UTC	1.30e-02	-1.38e-04	-8.25e-03	0.8829
ERS-12016-09-2202:34 UTC	1.99e-03	-5.99e-04	5.09e-03	0.3149
Adeos-22016-09-2203:25 UTC	NO			NO

Table 4: Estimated rotational velocity vectors in ECI coordinates (01.January 2000 12:00 UT).

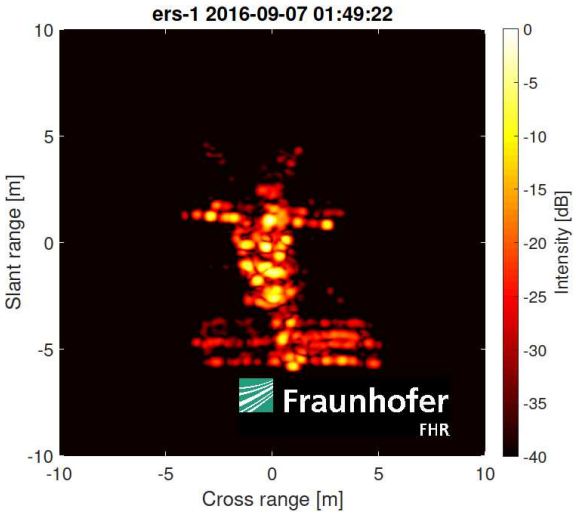

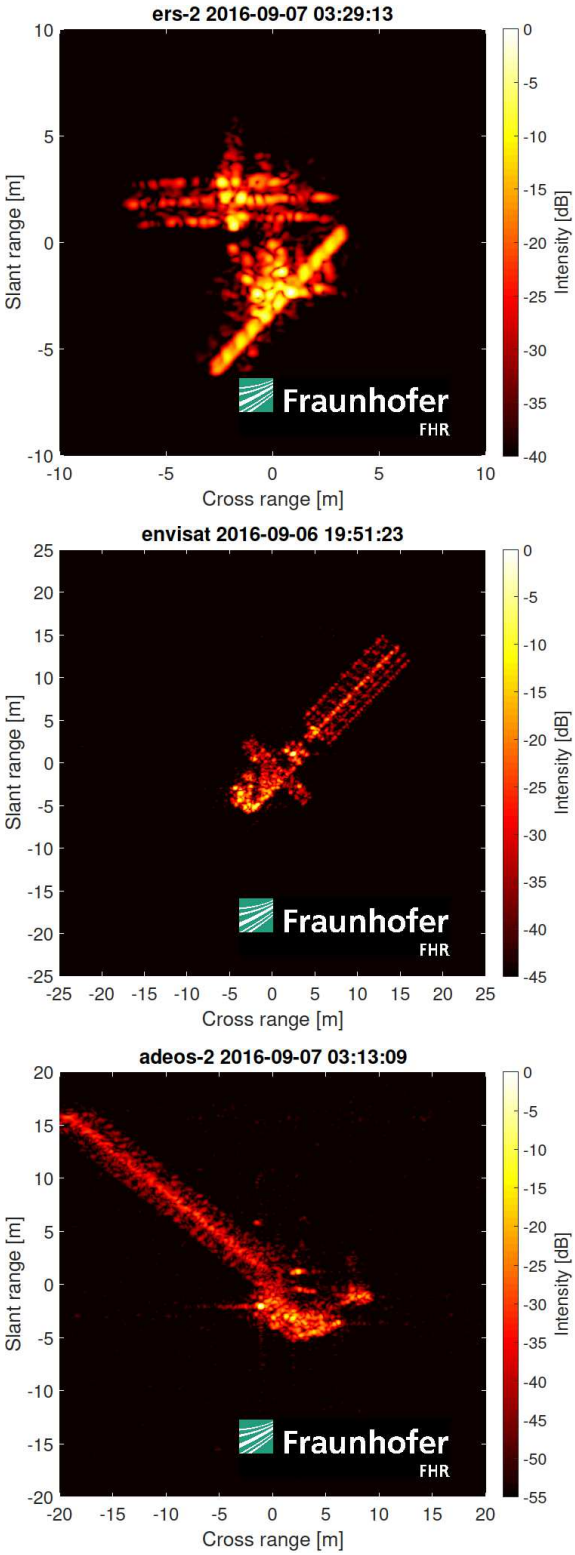

Figure 15. ISAR images of the observed satellites

7.4 Acquired measurements, ZIMLAT

7.4.1 Light curves

We acquired light curves for all priority targets during collaborative observation nights 2016-09-06 and 2016-09-21 (see Tab. 1 and 2). Light curves for satellites ENVISAT and ADEOS-2 acquired during night 2016-09-06 by ZIMLAT telescope are shown in Fig. 16. Light curves for both objects showed fast brightness variation over time. We processed both light curves in order to extract the apparent rotation period by applying method of epoch folding [8]. This method revealed that the apparent rotation period of ENVISAT was 192.4 s which corresponds to apparent rotation velocity 1.87 deg/s. For ADEOS-2 we got inconclusive results for apparent period, obtaining values between 45.6 s to 71.2 s where none of these numbers could be confirmed.

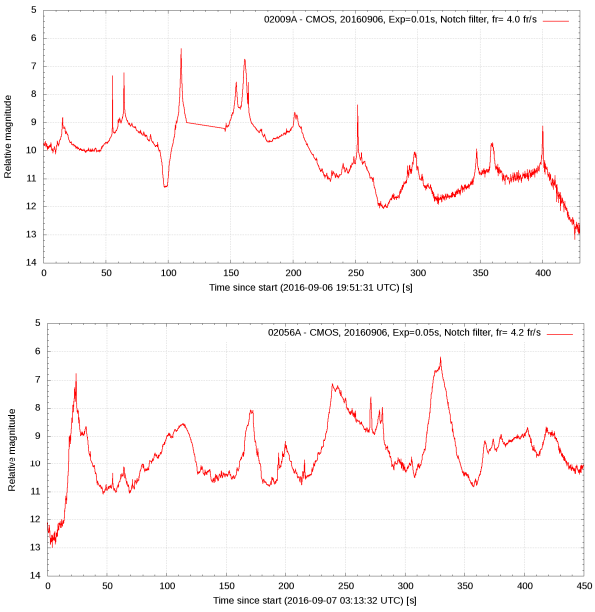

Figure 16. Light curve of ENVISAT (upper panel) and ADEOS-2 (lower panel) acquired during night 2016-09-06 by ZIMLAT telescope by using CMOS camera

7.4.2 SLR residuals

We were able to measure SLR residuals only for ENVISAT satellite during both collaborative observation nights. Example of our data is plotted in Fig. 17. The residuals showed a strong trend which was caused by the difference between the used predictions to track the object and its real position.

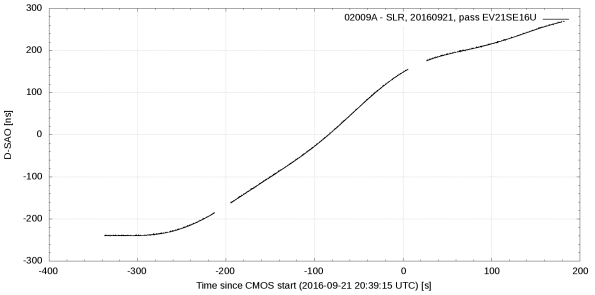

Figure 16. SLR residuals of ENVISAT acquired by ZIMLAT during night 2016-09-21

8 SUMMARY

In our work we presented an ESA study dedicated to the attitude determination of space debris objects such as defunct spacecraft and upper stages by using different types of observation techniques. Presented are acquisition and processing of the Inverse Synthetic Radar Images (ISAR), Satellite Laser Ranging (SLR) residuals and light curves.

There are in total four partners involved in the study each bringing a different expertise. The Hypersonic Technology Goettingen (HTG) (Germany) developed highly modular software tool ıOTA to model different types of measurement and to perform short-(days) and long-term (months, years) attitude predictions by assuming different torques and forces. Another partner, the Astronomic Institute of the University of Bern (AIUB) (Switzerland), which is a leader of the study, was responsible for the light curves and SLR residuals acquisition and processing. Similar expertise was covered by third partner the Space Research Institute's (IWF) (Austria). The forth partner the Fraunhofer Institute for High Frequency Physics and Radar Techniques FHR (Germany) is responsible for the acquisition and processing of radar data.

Five targets have been selected during our study for observations and attitude determination, namely satellites ENVISAT, ERS-1, ERS-1, ADEOS-2 and upper stage H-2A R/B. To four of them, LEO satellites, collaborative observations have been performed during two nights in September 2016 when ISAR images have been acquired by FHR's TIRA system along with the light curves acquired by AIUB's ZIMLAT telescope. We were able to measure SLR residuals for ENVISAT satellite only.

Finally, an analysis of ISAR images has been performed by FHR to determine the attitude states of all observed objects. Attitude states could be found for ENVISAT, ERS-1 and ERS-2. However, ADEOS-2 showed quite tumbling behaviour, which was also observed in the light curves by the ZIMLAT telescope.

Our next step is to fully processed the acquired data during collaborative campaign and further validate the ıOTA tool and its individual modules.

9 REFERENCES

1. Kanzler, R., Schildknecht, T., Lips, T., Fritsche, B., Silha, J., Krag, H., *Space Debris Attitude Simulation - ıOTA (In-Orbit Tumbling Analysis)*, Proceedings of the Advanced Maui Optical and Space Surveillance Technologies Conference, held in Wailea, Maui, Hawaii, September 15-18, 2014.

2. Silha, J., Schildknecht, T., Pittet, J.-N., Bodenmann, D., Kanzler, R., Karrang, P., Krag, H., *Comparison of ENVISAT's attitude simulation and real optical and SLR observations in order to refine the satellite attitude model,* Proceedings of AMOS Conference, Maui, Hawaii, 2016, (AIUB).

3. J.-N. Pittet, J. Silha, T. Schildknecht, *Single pass attitude determination of ENVISAT satellite trough the laser ranging measurements*, Advances in Space Research, *in preparation*

4. Kucharski, D., Kirchner, G., Koidl, F., Cunbo Fan, Carman, R., Moore, C., Dmytrotsa, A., Ploner, M., Bianco, G., Medvedskij, M., Makeyev, A., Appleby, G., Suzuki, M., Torre, J.-M., Zhang Zhongping, Grunwaldt, L., Qu Feng, *Attitude and Spin Period of Space Debris Envisat Measured by Satellite Laser Ranging IEEE transactions on geoscience and remote sensing*, 12, 7651-7657, 2014.

5. S. Sommer, J. Rosebrock, D. Cerutti-Maori, and L. Leushacke (2017). *Temporal analysis of ENVISAT's rotational motion*, 7th European Conference on Space Debris, ESA/ESOC, Darmstadt/Germany.

6. Dantowitz, R., *Sharper Images Trough Video*, Sky & Telescope, 96, No. 2 (August), 48-54, 1998.

7. J. Silha, T. Schildknecht, J.N. Pittet, A. Rachman, M. Hamara, *Extensive light curve database of Astronomical Institute of the University of Bern*, Proceedings of 7th European Conference on Space Debris, Darmstadt, Germany, 2017.

8. J. Silha, Linder E., Hager M., Schildknecht T., *Optical Light Curve Observations to Determine Attitude States of Space Debris*, Proceedings of 30th International Symposium on Space Technology and Science, Kobe-Hyogo, Japan, 2015.

9. M. Steindorfer, G. Kirchner, F. Koidl, P. Wang, *Light Curve Measurements with Single Photon Counters at Graz SLR*, Presented at Matera 2015 ILRS Technical Workshop, Italy, 2015.

10. K. Merz, D. Banka, R. Jehn, M. Landgraf, J. Rosebrock (2005). Observations ofinterplanetary meteoroids with TIRA, *Planetary and Space Science*, **53**, 1121–1134.

11. D. Mehrholz. (1996). Ein Verfolgungs- und Abbildungsradarsystemzur Beobachtung von Weltraumobjekten, *Frequenz*, 50:138–146, July 1996. doi:10.1515/FREQ.1996.50.7-8.138.